ADVANCED FUNCTIONAL MATERIALS
www.afm-journal.de

Check for updates

High-Gain Chemically Gated Organic Electrochemical Transistor

Siew Ting Melissa Tan, Alexander Giovannitti, Armantas Melianas, Maximilian Moser, Benjamin L. Cotts, Devan Singh, Iain McCulloch, and Alberto Salleo**

Organic electrochemical transistors (OECTs) have exhibited promising performance as transducers and amplifiers of low potentials due to their exceptional transconductance, enabled by the volumetric charging of organic mixed ionic/electronic conductors (OMIECs) employed as the channel material. OECT performance in aqueous electrolytes as well as the OMIECs' redox activity has spurred a myriad of studies employing OECTs as chemical transducers. However, the OECT's large (potentiometrically derived) transconductance is not fully leveraged in common approaches that directly conduct chemical reactions amperometrically within the OECT electrolyte with direct charge transfer between the analyte and the OMIEC, which results in sub-unity transduction of gate to drain current. Hence, amperometric OECTs do not truly display current gains in the traditional sense, falling short of the expected transistor performance. This study demonstrates an alternative device architecture that separates chemical transduction and amplification processes on two different electrochemical cells. This approach fully utilizes the OECT's large transconductance to achieve current gains of 10^3 and current modulations of four orders of magnitude. This transduction mechanism represents a general approach enabling high-gain chemical OECT transducers.

1. Introduction

Organic mixed ionic/electronic conductors (OMIECs) are effective transducers of chemical to electronic signals because their conductivity can be modulated by both electrochemical redox and chemical reactions. OMIECs are often conjugated polymers, designed to have appropriate energy levels to perform these reactions under ambient conditions. Judicious side chain engineering[1–7] or blending with polyelectrolytes facilitates mass transport in aqueous environments to successfully interface with biological systems.[8] These unique properties enable their application in electrochemical devices, including biosensors,[9–12] actuators,[13] energy storage materials,[14] transistors,[15] or neuromorphic devices.[16]

The organic electrochemical transistors (OECTs) (**Figure 1**a) leverage OMIECs' properties by utilizing them as the channel material, immersed in an electrolyte that provides ionic charge carriers. The OECT's gate electrode is often a non-polarizable pseudo-reference electrode, commonly a Ag/AgCl pellet electrode (a sintered blend of Ag and AgCl) that is immersed in an aqueous electrolyte.[17] The typical potentiometric operation of the OECT (Figure 1a) involves application of an external gate potential (V_G) between the gate and the channel (source). This potential induces a capacitive faradaic electron-transfer reaction between the source/drain eletrodes and the OMIEC[18] to modulate the OMIEC's electronic conductivity, which is probed by measuring the drain current (I_D) upon application of a drain bias (V_D). During this ET reaction, ions simultaneously migrate into the OMIEC and compensate the electronic charge carriers injected from the electrodes.[19] Concurrently, opposite non-capacitive faradaic redox reactions occur at the Ag/AgCl pellet ($Ag^0 + Cl^- \rightarrow AgCl + e^-$) to compensate for the change in ion concentration in the electrolyte and, consequently, to complete the electronic circuit. In most cases, where [Cl^-] is high enough to be considered virtually constant under the small perturbations occurring during OECT operation, the Ag/AgCl gate electrode maintains an approximately fixed potential such that V_G is imposed predominantly on the channel, enabling control of the charge state of the OMIEC channel. Using a gate electrode with a defined redox-potential such as the Ag/AgCl pellet allows reproducible determination of the OECT threshold voltage (V_T) crucial for benchmarking materials. Conversely, as the work function of redox-active conjugated polymers varies with their state of charge,[20] using polarizable OMIECs as the gate electrode causes the V_T to vary with the gate material and its processing history. This makes quantitative comparisons and benchmarking between different OECT channel materials nearly impossible.[13] It should be emphasized that in the ideal OECT operation, no ET reaction occurs between the channel

S. T. M. Tan, Dr. A. Giovannitti, Dr. A. Melianas, Dr. B. L. Cotts, D. Singh, Prof. A. Salleo
Department of Materials Science and Engineering
Stanford University
California 94305, USA
E-mail: ag19@stanford.edu; asalleo@stanford.edu
M. Moser, Prof. I. McCulloch
Department of Chemistry
Chemistry Research Laboratory
University of Oxford
Oxford OX1 3TA, UK
Prof. I. McCulloch
Physical Science and Engineering Division
King Abdullah University of Science and Technology
Thuwal 23955-6900, Saudi Arabia
The ORCID identification number(s) for the author(s) of this article can be found under https://doi.org/10.1002/adfm.202010868.

DOI: 10.1002/adfm.202010868

 © 2021 Wiley-VCH GmbH

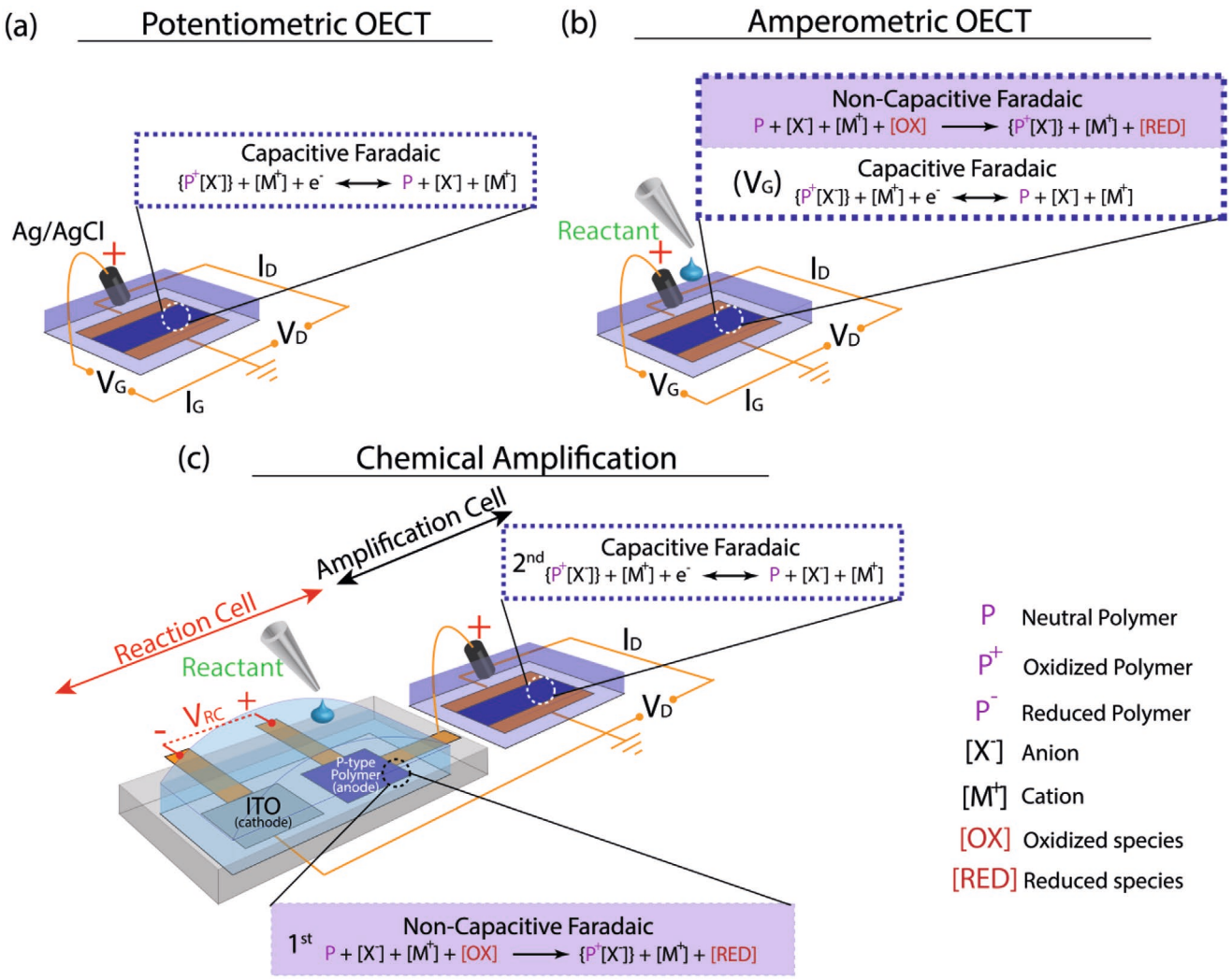

Figure 1. Comparison between operational modes of OECTs. a) Regular potentiometric operation of an OECT. An external power source applies a gate potential (V_G) to drive electrochemical reactions of the OMIEC channel material with respect to the gate electrode (Ag/AgCl pellet). This results in charging/discharging via non-capacitive faradaic reactions on the gate electrode and capacitive faradaic reactions of the OECT channel material, resulting in a change in OMIEC's conductivity. b) Amperometric operation of an OECT. An external V_G is applied to control the initial channel conductivity (capacitive faradaic reactions). Additionally, a redox-active reactant is introduced within the OECT electrolyte to enable exergonic or bias-dependent reactions with the OECT channel material (non-capacitive faradaic reactions). The Ag/AgCl gate pellet electrode undergoes redox-reactions to provide electronic charge carriers for charging and discharging of the OECT channel material and for faradaic side reactions with the analyte. c) Chemically enabled potentiometric operation of an OECT transducer. The redox-active analyte is added to a separate electrochemical cell (RC) where its electrodes are redox-active (i.e., RC anode). The redox-active materials are designed to spontaneously undergo electron transfer reaction with the analyte (via non-capacitive faradaic reactions), resulting in the charging/discharging of the electrode (oxidation/reduction). The change of the state of charge of the electrodes generates a potential across the RC with respect to the counter electrode (cathode) (e.g., ITO counter electrode) (referred to as V_{RC}). The change in V_{RC} is utilized to operate the OECT potentiometrically in a similar fashion as (a) by connecting the RC anode to the Ag/AgCl gate electrode of the OECT.

and the electrolyte. In practice however, parasitic side reactions such as the ET reaction from the OMIEC to ambient molecular oxygen (oxygen reduction reaction, ORR) are commonly observed for electron-rich OMIECs.[19]

While the basic operating principle is the same, one advantage of the OECT over the electrolyte-gated organic field-effect transistor is due to the ability of its channel to undergo volumetric charging (capacitive faradaic). Volumetric charging of the OMIEC results in a large transconductance $\left(g_m = \frac{\partial I_D}{\partial V_G}\right)$,[17,21] enabling amplification of minute perturbations in gate potential (∂V_G) into large modulations in drain current (∂I_D). The performance of OECTs can be optimized by maximizing their g_m through careful materials choice[17,21–23] as well as device design.[17,24–26]

The OECT's large g_m and unique properties of OMIECs have spurred the development of OECT-based sensors that can operate either potentiometrically or amperometrically. Potentiometric OECT sensors (Figure 1a) fully leverage the large g_m of the OECT. Indeed they have been used to transduce and

© 2021 Wiley-VCH GmbH

amplify weak biological potentials (∂V_G) into large modulations in channel conductance $\left(\frac{\partial I_D}{V_D}\right)$ in electroencephalography,[25] electrocorticography,[9,27] and electrocardiography[28] experiments. Alternatively, an OECT sensor can be operated amperometrically (Figure 1b) to detect redox-active analytes present in its electrolyte. The device is operated by applying a fixed V_G while monitoring changes of I_D after the addition of redox-active analytes.[29–32] The sensing mechanism relies on an ET reaction between the redox-active analyte and the OMIEC (non-capacitive faradaic redox reactions) to generate a measurable current, where the reaction rate is dependent on the applied V_G. The appeal of this approach is that it may allow to combine the chemical transduction capabilities of the OMIEC with the OECT's amplification properties, yielding a compact device architecture for sensitive biochemical sensing, such as the detection of biomarkers for early disease indication facilitated by analyte-specific enzymatic redox reactions.[29–31,33,34]

While without a doubt using the OECT as an amperometric sensor (which we subsequently refer to as A-OECT) enables the chemical transduction, its electronic amplification has been questioned.[35] Indeed, to maintain charge neutrality in the electrolyte, the following redox equilibrium of Ag/AgCl ($Ag^0 + Cl^- \rightarrow AgCl + e^-$) will result in current gains $\left(G = \frac{\Delta I_D}{\Delta I_G}\right)$ of ≈1. For instance, ET between the analyte and the channel, in the case of channel oxidation, will result in an unbalanced positive charge in the electrolyte, which is compensated by the injection of Cl^- from the Ag/AgCl gate electrode via the addition of an equal number of electrons at that electrode. Thus when a non-polarizable Ag/AgCl gate electrode is used, the reaction current due to ET on the channel $(\Delta I)_D$ is compensated by a similar current through the gate electrode $(\Delta I)_G$. Because charge balance in the electrolyte is a general principle, the same argument applies if the gate electrode is a polarizable OMIEC, with the added complication that in this case the gate electrochemical potential may vary as ET proceeds on the gate, making the link between I_D and analyte concentration more complex. Furthermore, air-sensitive OMIECs such as the commonly used PEDOT:PSS readily undergo parasitic side reactions with ambient redox-active molecules such as molecular oxygen (ORR), which are additionally voltage-dependent, which add to the currents generated by the analyte of interest interfering with sensor accuracy.[19]

Within the context of biosensing, it is often important to be able to measure low currents reliably. First and foremost, detecting low currents enables detection of low analyte concentrations. Furthermore, while it is attractive to rely on a direct ET reaction between an enzyme and the OMIEC channel to avoid electron mediators, this advantage often comes at a price in terms of current.[30,34] Indeed, achieving direct ET is notoriously challenging as it requires careful alignment between the electronic energy levels of the OMIEC and the redox-active center of the enzyme (e.g., the co-factor flavin adenine dinucleotide (FAD) in glucose oxidase for glucose sensing).[36,37] Imperfect alignment of the energy levels results in low detection efficiency and consequently low reaction currents.[34] While controlling V_G may enhance these ET reaction currents, it may additionally exacerbate currents generated by undesirable parasitic reactions such as the ORR thereby degrading the sensing signal and sensor accuracy.

Measuring low reaction currents using OECTs is problematic because the most common OECTs are PEDOT:PSS-based and thus operate in depletion mode. Indeed, while the OECT's large g_m is frequently quoted as a premise for amperometric OECT operation, the amperometric approach results in sub-unity amplification as explained above and also shown by Macchia et. al.,[35] thus failing to capitalize on the OECT transistor action. When a depletion mode OECT is operated above-threshold, especially at maximum g_m, the channel is initially highly conductive, resulting in large $(I_0)_D$. Hence, measuring a ΔI_D—that remains small due to the lack of amplification—over a large baseline of $(I_0)_D$ is challenging, especially when ambient/instrument noise is of similar magnitude as ΔI_D. This observation led to the development of enhancement mode OECTs for amperometric sensing.[30] These devices allowed measurement of currents as low as a few nAs to tens of nAs, however these low currents suggest very weak amplification, if any at all.

To mitigate these issues, Macchia et al. proposed a hypothetical amperometric bipolar junction transistor OECT structure where redox reaction currents on the base (gate) would be amplified into collector–emitter (source–drain) current.[35] Another approach would be to utilize a polarizable OMIEC-based gate electrode where the ET reaction is limited to the gate, allowing the gate's work function, and V_T, to shift.[11] While this design circumvents some of the limitations of operating OECTs amperometrically, it remains suboptimal for sensing. For instance, as the ET reaction is conducted in an electrolyte shared by both the gate and channel, diffusion of redox-active species may lead to additional unintended side reactions on either the channel, the gate, or both. Furthermore, to obtain the maximum potential change at the gate requires a small gate capacitance, which in turn is detrimental to effective channel gating, thus resulting in a device with intrinsically conflicting design requirements between sensing and amplification.

In this work, we demonstrate a proof of concept high-gain chemical transducer which operates the OECT potentiometrically. By physically locating the faradaic redox reaction of the analyte on a reaction cell (RC) separate from the OECT, our approach first transduces the reaction into a potential (V_{RC}) that is subsequently amplified by the OECT (Figure 1c). We take advantage of the basic engineering principle of electrically connecting separate components each optimized to perform the single function that is required of them. As a result, we eliminate many of the design trade-offs that are introduced when a single device must perform multiple functions (e.g., sense and amplify), which typically lead to non optimal performance, as described above. Remote[38–40] and extended gate[41,42] transistors are examples of devices that employ this simple engineering design principle. While the same design heuristic is employed in designing the RC-OECT, the operation mechanism is fundamentally different. Detection mechanisms in the remote and extended gates involve capacitive processes while the RC transduces non-capacitive faradaic charge transfer reactions of redox-active analytes. Additionally, the mechanism of potentiometric amplification of the RC-OECT is distinct from

© 2021 Wiley-VCH GmbH

regular potentiometric sensors[43,44] which are purely capacitive in nature.

We demonstrate the working principle of our device for the detection of a model redox-active molecule H_2O_2, a common analyte detected in electrochemical sensors[45] as an abundant intermediate in biological environments[46] and oxidoreductase enzymatic reactions (e.g., glucose, lactate, and ethanol).[47,48] Comparing the performance of our potentiometrically operated device to an amperometric OECT, we bring to light the most salient pitfalls inherent to operating OECTs amperometrically. We stress that our goal is not to showcase record-breaking sensitivity in a sensor but rather describe the general principles and operation mechanism of a potentiometric OECT as a high-gain transducer of ET reactions, which we propose as a more efficient alternative to all-in-one devices performing the same function.

2. Results

Figure 1c illustrates our device's architecture where the two electrochemical cells (RC and OECT) are physically separate but electrically connected. Unlike a conventional OECT where an external source meter unit (SMU) provides V_G, in our device V_G is generated by a chemical reaction between the redox-active analyte and electrodes within a two-electrode RC. The RC's primary electrode is comprised of a redox-active OMIEC deposited on a conductive indium doped tin oxide (ITO) substrate, which is in electrical contact with the non-polarizable gate electrode (Ag/AgCl pellet) that is immersed in a separate electrolyte to gate the OECT. The RC's counter electrode shares a common ground with the OECT source electrode. Upon addition of the redox-active species to the RC electrolyte, the ET reactions with the RC electrode results in a change in its potential, which gates the OECT ($V_{RC} = V_G$).

Utilizing a non-polarizable gate electrode results in an equivalent change in potential of the OECT channel and hence a change in its charge density and conductivity. Separating the RC from the OECT allows us to choose the redox-active OMIEC with the highest activity toward the ET reaction without having to simultaneously ensure that it is an effective gate material for the OECT. Furthermore, we can make certain that the ET reaction generates the largest potential change by using a small capacitance electrode, which would pose a design challenge if the same electrode were to be used as the OECT gate. These arguments illustrate the instrinsic advantage of being able to optimize the RC separately from the OECT. As an added benefit, the generation of V_G eliminates the need for an external power supply to control V_G, enabling chemically powered sensors.

To demonstrate this concept, we utilize H_2O_2 as the redox-active species, over a concentration range on the order of 0.1 to 10 mM. The RC primary electrode, hereafter termed the RC anode, is a *p*-type conjugated polymer OMIEC based on 3,3′-dialkoxybithiophenes (p(gT2))[14] which has a high reactivity for the hydrogen peroxide reduction reaction (HPRR) that oxidizes the RC anode while converting H_2O_2 to H_2O (Figure S1, Supporting Information). To study the simplest RC-OECT configuration, and to conduct HPRR solely on the RC anode, a bare ITO electrode with low HPRR catalytic activity is utilized as the counter electrode of the RC (cathode). The RC and OECT, while physically separate, both contain Phosphate Buffered Saline (PBS) solution as the electrolyte to maintain a constant pH. During the operation of the device, H_2O_2 is added to the RC electrolyte, triggering HPRR to oxidize the RC anode which increases V_{RC}. The increase in gate potential is subsequently employed to turn a *p*-type OECT (p(gT2) as channel (Figure S2, Supporting Information),[5] which we operate in depletion mode, from an ON to OFF state.

To effectively compare the performance of the proposed RC-OECT to that of an amperometric OECT, p(gT2) is utilized both as the redox-active OECT channel material (**Figures** 1b and 2c) and as the RC anode in the potentiometric RC-OECT design (Figures 1c and 2b). Additionally, H_2O_2 of identical concentrations are added to the RC and A-OECT electrolyte, respectively. Figure 2a shows the response of the RC-OECT (schematic in Figure 1c) after the addition of H_2O_2 to the RC at 60 s. The rapid rise in V_{RC} corresponds to the oxidation of the p(gT2) anode by HPRR, turning off the OECT and thus leading to a concomitant drop in I_D.

To verify the efficacy of gating the OECT by the reaction in the RC, the expected I_D (Figure 2a, red dotted line) is calculated based on the time-varying evolution in V_{RC} (blue dashed line) and the OECT transfer curve (Figure 2b). The close agreement between the predicted and empirical ΔI_D indicates that the RC-OECT exhibits the expected amplification properties of the OECT, that is, the potential change on the RC (ΔV_{RC}) indeed induces similar modulation as would an externally applied V_G by an SMU. This result also confirms that the power output (≈0.1 μW) from the RC's chemical reaction is sufficient to gate the OECT.

To maximize RC-OECT response (i.e., magnitude of ΔI_D), the range of potential change across the RC ($V_{RC(initial)}$ to $V_{RC(final)}$) should have large overlap with the potential range where the OECT exhibits the largest g_m. Figure 2b shows the transfer curve of the OECT, where ΔV_{RC} (–0.08 V to + 0.05 V, shaded region) overlaps with maximum g_m, enabling the RC-OECT to achieve current modulation (ΔI_D) on the order of 1 mA. The RC-OECT exhibits 0.1–1 mA of drain current modulation over H_2O_2 concentration range spanning three orders of magnitude while retaining high efficacy of transducing a potential change ($R^2 = 0.95$) into drain current modulation ($R^2 = 0.94$) (Figures S3 and S4, Supporting Information). Furthermore, the usage of a non-polarizable Ag/AgCl pellet instead of a metal or OMIEC as the gate electrode enables stable and reproducible operation of the RC-OECT (Figure S5, Supporting Information). These results demonstrate that the potentiometric operation of the RC-OECT effectively utilizes the OECT's unique strength, that is, large transconductance.

This amplification is not observed during the operation of the amperometric OECT (Figure 2c). Increasing V_G from –0.4 to + 0.3 V versus Ag/AgCl modulates the pristine OECT from the ON to OFF state (with OFF currents ≈45 nA), with low gate currents (on the order of 10 nA). After the addition of H_2O_2, large HPRR reaction currents $(\Delta I)_G$ on the order of 100 nA are observed at $V_G > + 0.1$ V due to the enhanced reactivity of p(gT2) for HPRR at increasingly positive gate potentials (Figure S6a, Supporting Information). This reaction increases

© 2021 Wiley-VCH GmbH

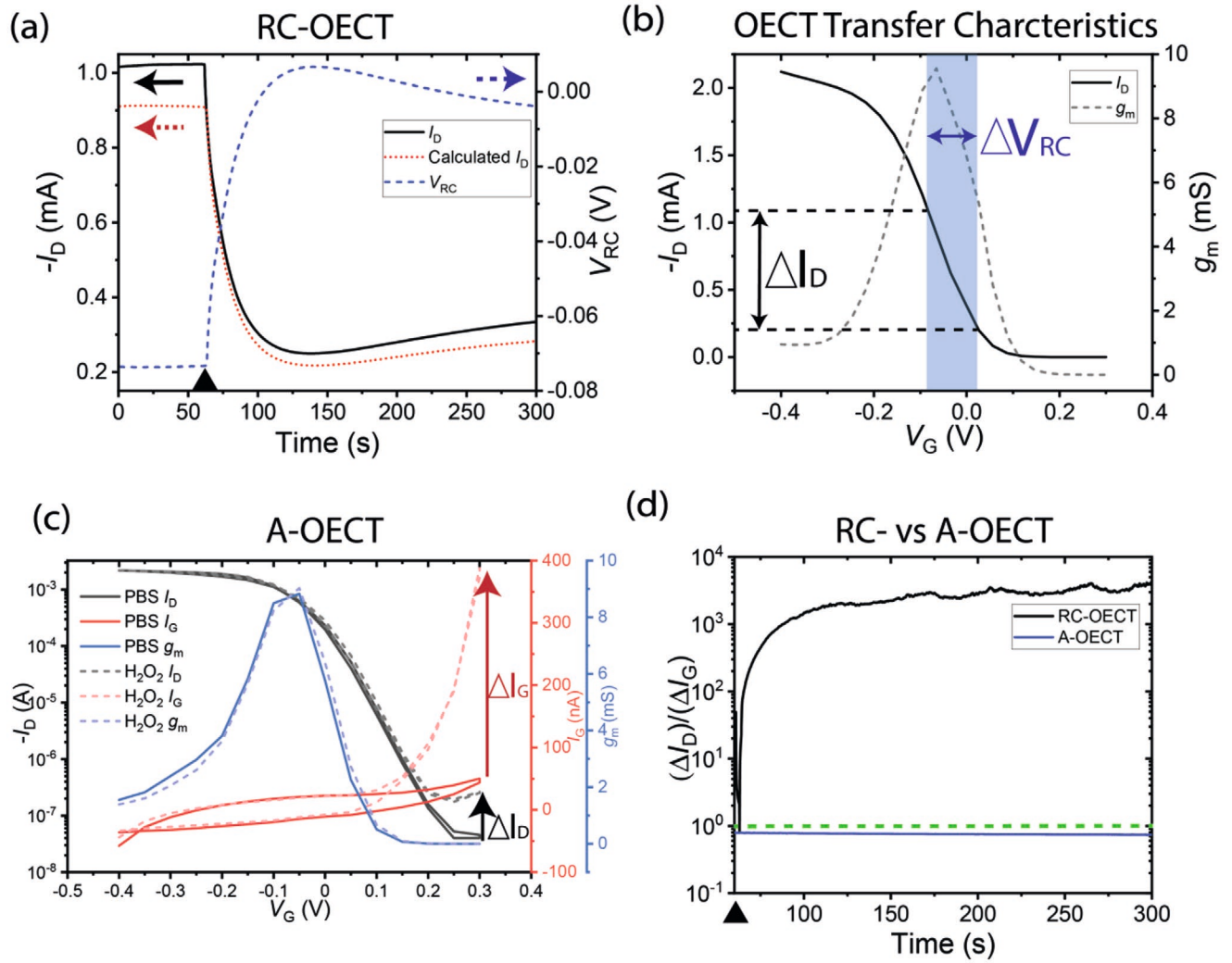

Figure 2. Operation of the RC-OECT and A-OECT in presence of model redox-active analyte H_2O_2. a) Operation of the RC-OECT (schematic shown in Figure 1c) with PBS as the supporting electrolyte for both OECT and RC. H_2O_2 (33 mM) is added to the RC (indicated by triangle) at $t = 60$ s. The I_D (OECT) (black line) and the V_{RC} (RC) (blue dashed line) are monitored for 5 mins. The calculated I_D based on the OECT transfer curve is depicted as a red dotted line. See Figure S11, Supporting Information, for calculation approach. b) Transfer curve of the OECT (black solid curve) and transconductance (grey dotted line) ($V_D = -0.1$ V). The potential range of the RC (ΔV_{RC}) highlighted (blue box) and corresponding ΔI_D. c) Operation of the amperometric OECT with PBS, showing the transfer curve of the OECT with p(gT2) as the channel material ($V_D = -0.1$ V). The I_D (black line), I_G (red line), and g_m (blue line) are shown before (solid lines) and after the addition of 33 mM H_2O_2 to the OECT electrolyte (dashed lines). The red arrow shows the increase in I_G beginning at $V_G > 0$ V due to faradaic side reactions (HPRR) of the OECT channel material and H_2O_2. An additional increase in I_D is observed after the addition of H_2O_2. Accelerated HPRR occurs at V_G different from the range of maximum g_m d) Ratio of drain current modulation (ΔI_D) with respect to reaction or gate current modulation (ΔI_G) of RC-OECT (black trace) versus amperometric OECT at $V_G = +0.3$ V (blue trace). Triangle indicates addition of 33 mM H_2O_2 to electrolyte of RC or electrolyte of amperometric OECT, respectively. Green dotted line indicates ratio of unity. See Figure S9b, Supporting Information, for ΔI_D and ΔI_G.

the OECT OFF current (I_D), and, as expected on basis of charge conservation, results in $(\Delta I)_D \approx (\Delta I)_G$.

Since $(\Delta I)_D$ is limited by the reaction current $(\Delta I)_G$, which is ultimately limited by the analyte concentration, measuring such small currents (≈100 nA) requires minimizing the baseline current I_0. In this case the most optimal operation of the A-OECT occurs at a gate potential where the OECT is in the subthreshold regime and HPRR is accelerated. The low initial OFF currents (I_0) at $V_G = +0.3$ V enables a fractional response $(\Delta I/I_0)_D$ of ≈1.5, better than or comparable to other A-OECT examples in literature[11,29,30,34] (Figure S6b,c, Supporting Information). However, Figure 2c shows that while operating the amperometric OECT at $V_G = +0.3$ V exhibits the best fractional response, it does not overlap with peak OECT transconductance ($V_G = -0.1$ V) and is in fact where the OECT exhibits the lowest transconductance. If the A-OECT is operated at peak transconductance, the small $(\Delta I)_D$ would barely be measurable over the large baseline signal I_0 resulting in a negligible fractional response (Figure S6b, Supporting Information). Hence, the optimal operation of the A-OECT from the standpoint of signal-to-noise does not take advantage of the OECT's large transconductance, which is optimized by channel material

© 2021 Wiley-VCH GmbH

choice and device geometry. Rather, the A-OECT functions more as a redox-active electrode for ET reactions than a transistor (Figure S7, Supporting Information).

Even though our A-OECT is on par or better with the best literature examples in terms of fractional response, the effective leverage of OECT transconductance in our RC-OECT results in significantly superior amplification. To effectively compare the amplification abilities of the A-OECT and RC-OECT, current gain $G = \frac{\Delta I_D}{\Delta I_G}$, the ratio of measured drain current response over the input analyte faradaic current, is compared. Indeed, the RC-OECT exhibits current gains $G = \frac{\Delta I_D}{\Delta I_G}$ on the order of 10^3 (Figure 2d and Figure S8a, Supporting Information). Despite a lower reaction current density generated by the RC of ≈1 μA cm^{-2} compared to the A-OECT's ≈500 μA cm^{-2} (which we note is also enhanced by actively biasing V_G at the risk of enabling parasitic side-reactions), we obtain a ΔI_D ≈1 mA at a V_D = −0.1 V in the connected OECT (black trace in Figure S9b, Supporting Information). This is the result of utilizing the RC's potential change (ΔV_{RC} ≈ + 0.1 V that overlaps with max g_m) to gate the OECT thus amplifying the reaction current by 10^3. On the other hand, since the A-OECT's ΔI_G and ΔI_D are of similar magnitude (Figure S9a, Supporting Information), the current gains (Figure 2d and Figure S8a, Supporting Information) and amplification factors $\left(\frac{(\Delta I / I_0)_D}{(\Delta I / I_0)_G}\right)$ (Figure S6c, Supporting Information) are below unity. Over a concentration range of three orders of magnitude, the sensitivity of the A-OECT is 23.8 μA M^{-1} while that of the RC-OECT is 0.24 mA Dec^{-1} (Figure S7, Supporting Information). Furthermore, as H_2O_2 concentration is minimized, the faradaic reaction currents approach the noise floor of the measurement instrument (nA), rendering it extremely challenging to measure low concentrations accurately. Hence, the superior performance and utility of the RC-OECT becomes more pronounced at lower concentrations of H_2O_2, where it exhibits drain current modulations of four to five orders of magnitude greater than the A-OECT (Figure S8b, Supporting Information). Hence, operating the RC-OECT potentiometrically truly utilizes the OECT as an amplifier and enhances the RC's performance as an electrochemical transducer.

To further improve the performance of the proposed RC-OECT, the range of V_{RC} can be widened so that it not only encompasses gate potentials at which the OECT exhibits maximum g_m but also the subthreshold region for maximum current modulation ratios. This can be achieved by functionalizing the RC cathode with an electron acceptor to facilitate direct ET from the analyte to the cathode. The ability to functionalize the counter electrode on the RC provides additional flexibility in RC-OECT optimization over that of the OECT which is limited to two redox active electrodes (gate and channel), which additionally have other constraints. We demonstrate this concept by utilizing a model oxidoreductase enzymatic reaction of glucose and glucose oxidase (GOx) that is a common reaction utilized in electrochemical sensors.[49,50] This reaction is conducted in the PBS electrolyte of the RC and the RC cathode is functionalized with tetrathiafulvene tetracyanoquinodimethane (TTF-TCNQ) (**Figure 3**a). TTF-TCNQ (Figure S10, Supporting Information) was selected because its electron affinity is larger than that of the $FADH_2$ co-factor of GOx to enable direct ET from $FADH_2$ to the functionalized cathode (Figure 3b, pathway 1).[37] Furthermore, oxidoreductase enzymes (e.g., GOx) form additional redox-active intermediates (e.g., H_2O_2),[47,48] which are intentionally generated to oxidize the anode p(gT2) via HPRR (Figure 3b, pathway 2).

As illustrated in Figure 3c, the combined effects of direct ET to TTF-TCNQ and oxidation of p(gT2) led to the bifunctionalized RC achieving an increased ΔV_{RC} > 300 mV, which is the sum of potential change from reduction of TTF-TCNQ and oxidation of p(gT2). This significant increase in ΔV_{RC} allowed the OECT to achieve current modulation ratios > 10^4 with low I_D OFF currents of 30 nA (Figure 3d). The improved performance of the bifunctionalized RC-OECT is due to the large overlap of ΔV_{RC} with the transfer curve (Figure 3d, inset). This large current modulation expands the detectable dynamic concentration range to span over additional orders of magnitude, improving the application range of OECT-based chemical detectors. For example, this expanded range would allow measurements of small relative analyte concentration changes over a large background concentration. Hence, by designing the RC and OECT individually as well as optimizing RC performance, the combined RC-OECT exhibits far superior performance over the A-OECT.

Finally, the modular design of the RC-OECT allows the OECT to be reused for multiple reactions by swapping in new RCs, improving cost and time effectiveness. By utilizing an air-reactive OMIEC as the OECT channel and operating in ambient conditions, the OECT's initial channel conductivity can be easily recovered by simply disconnecting the RC from the OECT to reset the OECT to I_D^0 (Figure S11, Supporting Information). We demonstrate this flexible modularity of our RC-OECT by employing it to transduce other H_2O_2-producing reactions such as the oxidoreductase enzymatic reactions of common biomolecules including lactate by lactate oxidase (LOx) and ethanol by alcohol oxidase (AlOx) (Figure S12, Supporting Information), paving the way for low-cost point-of-care diagnostics.

In summary, we demonstrate a chemically powered potentiometric OECT which fully utilizes the OECT's unique transistor properties to amplify reaction currents with a high gain. Separating sensing from amplification allows optimization of each component separately for best performance rather than having to find a compromise within a single device which is likely to be suboptimal in at least one of its functions. We utilize a RC to physically separate the chemical reaction of the redox-active analyte (e.g., H_2O_2) from the electrochemical operation of the OECT (amplification) instead of conducting sensing reactions in the same electrolyte as the OECT (amperometric operation, A-OECT). We elucidate the device operation mechanism and demonstrate the inherent advantage of potentiometric OECT sensors over conventional amperometric OECTs. Finally, we demonstrate the broad applicability of the device by utilizing enzymatic reactions to detect metabolites, achieving current modulations > 10^4, corresponding to a dynamic range of 40 dB, with low I_D OFF currents of 30 nA, utilizing the OECT's ON/OFF ratio. To our knowledge, such a large change in channel conductance has yet to be achieved by OECT-based

© 2021 Wiley-VCH GmbH

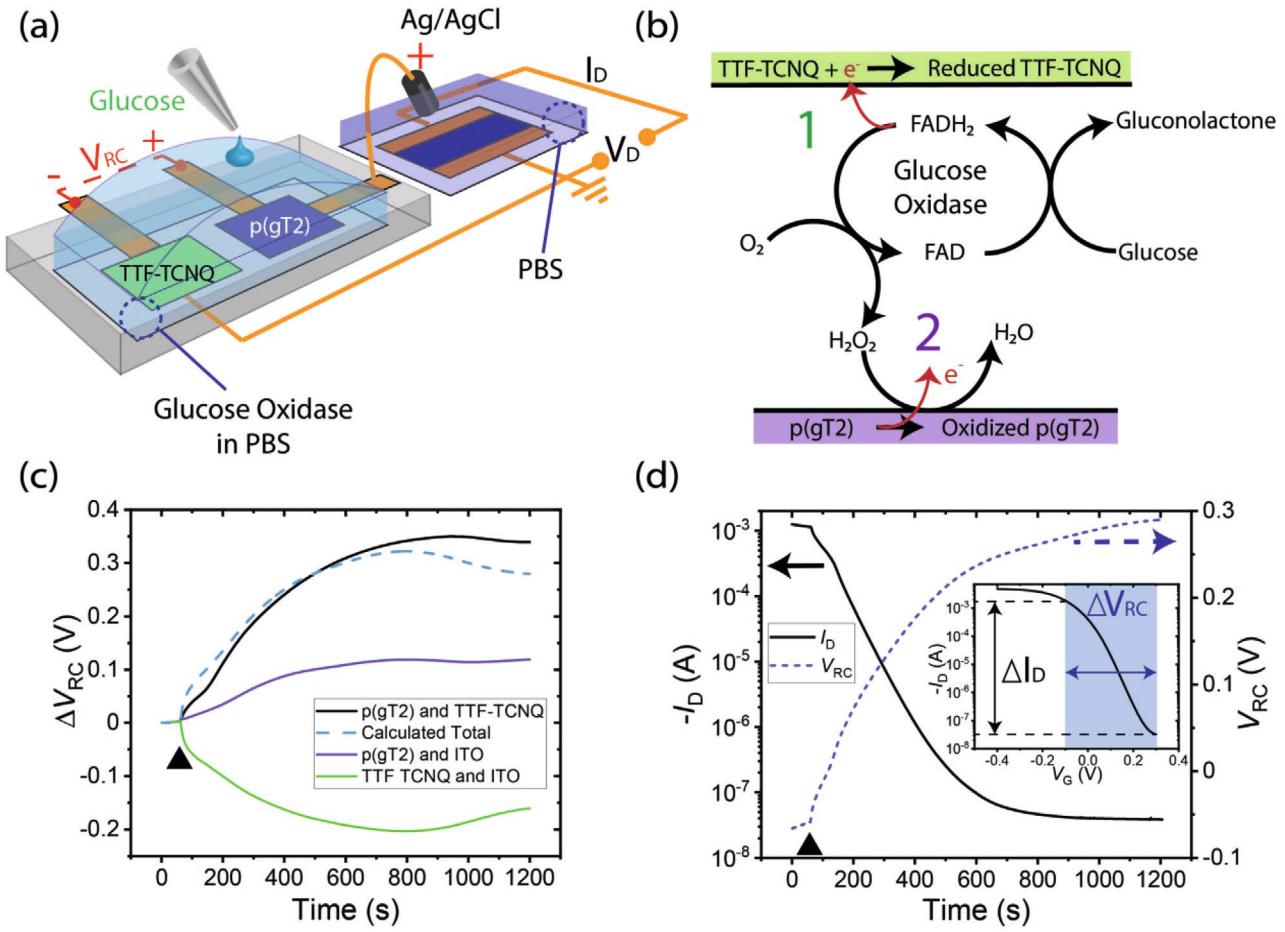

Figure 3. Operation of bi-functionalized RC with OECT. a) Schematic of RC-OECT with *p*-type polymer p(gT2) as anode and *n*-type electron collector TTF-TCNQ as cathode with PBS and GOx as the RC electrolyte. The OECT consists of p(gT2) as the channel material, Ag/AgCl pellet as gate electrode with PBS as electrolyte. The RC cathode shares a common ground with the source of the OECT. The RC anode is connected to the Ag/AgCl OECT gate electrode. b) Summary of the reactions occurring in the RC: 1) ET reaction (reduction) from the reduced GOx to TTF-TCNQ and 2) HPRR (oxidation) of p(gT2) by H_2O_2. c) Monitoring of the OCV of the RC (2-electrode measurements) for thin films containing p(gT2) (purple line) versus ITO, TTF-TCNQ (green line) versus ITO, the empirical combination of p(gT2) and TTF-TCNQ (black solid line) after the addition of glucose (33 mM) to GOx in PBS and the calculated sum of the OCV of the two individual electrodes (light blue dashed line). d) Detection of glucose using the RC-OECT. The OECT is operated by applying $V_D = -0.2$ V in PBS solution (ambient conditions). Glucose (33 mM) is added to a solution of GOx in the RC at $t = 60$ s, indicated by the triangle. The potential change across RC (V_{RC}) and I_D are monitored for 20 mins (V_{RC} (blue dashed line), I_D black solid line). The inset shows the transfer curve ($V_D = -0.2$ V, the blue rectangle highlights ΔV_{RC}).

chemical transducers. While the RC-OECT offers significant improvements in current gain compared to A-OECTs, the former's response time is slow compared to the latter. This can be addressed in future device design by further optimizing the RC by enzyme immobilization on the electrodes.[51,52] The relationship between I_D and H_2O_2 concentration was measured by sequential additions of increasing the concentration of H_2O_2 to the RC electrolyte over time (Figure S4, Supporting Information). This resulted in sequential decrease in I_D when increasing H_2O_2 concentration. We note that the recovery of the device is slow and further materials design is required to enhance the recovery time. Nevertheless, the RC is specifically designed to be modular and for one-time use. Hence, a fresh RC can be easily replaced while utilizing the same OECT for amplification.

Looking forward, with these improvements to the RC, we envision utilizing the device for the sensing of metabolites using enzymatic reactions in real-life applications. The ability to harvest energy from hydrogen peroxide, a common product in biological systems and enzymatic reactions, to power electrochemical devices demonstrates the generalizability of the RC-OECT to be powered by and transduce a range of biological reactions. We envision that these findings will spur further development of high-gain OECT-based devices by utilizing the proposed approach of separating chemical reactions from the transistor.

3. Experimental Section

Materials: Polymer p(gT2) was synthesized according to the literature.[14] Glucose oxidase (GOx) type II from *Aspergillus niger*, lactate oxidase (LOx) from *Aerococcus viridans*, and alcohol oxidase (AlOx) from Hansenula sp. were purchased from Sigma–Aldrich and stored at −20 °C. 30% H_2O_2 solution in H_2O was purchased from Sigma–Aldrich and stored at 4 °C. D-glucose, sodium lactate, and TTF-TCNQ

© 2021 Wiley-VCH GmbH

were purchased from Sigma–Aldrich. PDMS adhesives were purchased from 3M. 2 cm × 2 cm polished ITO coated glass slides for the RC were purchased from Xin Yang Technology Ltd.

RC Anode Preparation: p(gT2) was dissolved in chloroform at 10 mg mL^{-1} and spin coated on ITO/glass at 1000 rpm, and annealed at 60 °C for 10 minutes in ambient conditions to yield film thickness of 120 nm.

OECT Fabrication: Photolithographically patterned chips with gold contacts and patterned parylene to expose regions for the channel were used as OECT chips.[17] p(gT2) was dissolved in chloroform at 10 mg mL^{-1} and spin coated at 1000 rpm, annealed at 60 °C for 10 minutes, followed by parylene lift-off to form the channel. The OECT device dimensions were $L = 10$ µm, $W = 2$ mm, $d = 120$ nm and operated at $V_D = -0.1$ V for both the amperometric OECT and RC[p(gT2)/ITO]-OECT [p(gT2)].

Film Thickness Measurements: Thickness measurements were conducted on a DekTak 150 Surface Profiler using 1 mg tip force.

Enzyme Solutions: Enzyme solutions were prepared in the concentrations of 20.4, 2.4, and 14 mg mL^{-1} in PBS solution for GOx, LOx, and AlOx, respectively. Fresh solutions were prepared before each measurement.

Electrochemical Measurements: All electrochemical characterization of the RC anode or cathode were conducted using a 3-electrode setup with a saturated Ag/AgCl reference (BASi) and Pt mesh counter electrode on a Biologic SP-300. PDMS wells were adhered on the RC substrates to confine the reaction solution. For monitoring the open circuit potential between the polymer and Ag/AgCl reference using enzymatic reactions, 400 µL of enzyme solution was drop cast on the surface of the RC and 200 µL of 100 mM analyte added after 1 minute. For control measurements, 400 µL of PBS was drop cast and 200 µL of 100 mM H_2O_2 added after 1 minute. In chronoamperometry measurements, the potential of the working electrode was held at its initial open circuit potential and the current flow into the film measured during the above reactions. The scan rate for the cyclic-voltammogram measurements was 50 mV s^{-1} and conducted in PBS solution in ambient conditions unless stated otherwise.

TTF-TCNQ Cathode Preparation: 80 µL of a 40 mg mL^{-1} dispersion of TTF-TCNQ in acetonitrile was drop cast on an ITO/glass substrate and dried at ambient conditions overnight.

Two-Electrode RC Measurements: The potential between the *p*-type material anode or TTF-TCNQ and ITO was measured by placing the working electrode on the *p*-type anode or TTF-TCNQ and shorting the counter and reference leads to the ITO electrode. The potential between p(gT2) and TTF-TCNQ was recorded by placing the working electrode on p(gT2) and shorting the counter and reference to TTF-TCNQ.

OECT Measurements: Transfer and output characteristics of the OECTs were obtained using a custom LabVIEW program with a K2612 Keithley. PBS solution was used as the electrolyte and Ag/AgCl pellet as gate.

RC-OECT Measurements: The potential across the RC was monitored using a 2-electrode setup on a Biologic SP-300 with the working electrode on the polymer and the reference/counter electrode on the ITO counter electrode. The V_D across the OECT was supplied by a K2612 Keithley and I_D measured using a custom LabVIEW program. ITO counter electrode was functionalized by drop casting 80 µL of a 40 mg mL^{-1} dispersion of TTF-TCNQ in acetonitrile and dried at ambient conditions overnight.

A-OECT Measurements: Transfer and output characteristics of the OECTs were obtained using a custom LabVIEW program with a K2612 Keithley. PBS solution was used as the electrolyte and Ag/AgCl pellet as gate. A constant drain voltage ($V_D = -0.1$ V) and gate voltage (V_G ranging from −0.3 to +0.3 V) was applied. The drain and gate currents were measured simultaneously after addition of 100 µL 100 mM H_2O_2 to 200 µL of PBS electrolyte.

Supporting Information

Supporting Information is available from the Wiley Online Library or from the author.

Acknowledgements

The authors thank the Dionne lab for access to their UV–vis spectrometer and the Soft and Hybrid Materials Facility in the Stanford Nano Shared Facilities for access to the rheometer and profilometer. A.G. and A.S. acknowledge funding from the TomKat Center for Sustainable Energy at Stanford University. A.S. and M.T. gratefully acknowledge support from the National Science Foundation Award CBET #1804915. A.M. gratefully acknowledges support from the Knut and Alice Wallenberg Foundation (KAW 2016.0494) for Postdoctoral Research at Stanford University. Part of this work was performed at the Stanford Nano Shared Facilities (SNSF), supported by the National Science Foundation under award ECCS–1542152.

Conflict of Interest

The authors declare no conflict of interest.

Data Availability Statement

Research data are not shared.

Keywords

chemical to electrical transduction, electrochemistry, high gain transistors, organic mixed ionic/electronic conductors

Received: December 21, 2020
Revised: February 4, 2021
Published online:

[1] A. Giovannitti, C. B. Nielsen, D. T. Sbircea, S. Inal, M. Donahue, M. R. Niazi, D. A. Hanifi, A. Amassian, G. G. Malliaras, J. Rivnay, I. McCulloch, *Nat. Commun.* **2016**, *7*, 1.
[2] J. Mei, Z. Bao, *Chem. Mater.* **2014**, *26*, 604.
[3] A. Giovannitti, I. P. Maria, D. Hanifi, M. J. Donahue, D. Bryant, K. J. Barth, B. E. Makdah, A. Savva, D. Moia, M. Zetek, P. R. F. Barnes, O. G. Reid, S. Inal, G. Rumbles, G. G. Malliaras, J. Nelson, J. Rivnay, I. McCulloch, *Chem. Mater.* **2018**, *30*, 2945.
[4] J. F. Ponder, A. M. Österholm, J. R. Reynolds, *Chem. Mater.* **2017**, *29*, 4385.
[5] M. Moser, T. C. Hidalgo, J. Surgailis, J. Gladisch, S. Ghosh, R. Sheelamanthula, Q. Thiburce, A. Giovannitti, A. Salleo, N. Gasparini, A. Wadsworth, I. Zozoulenko, M. Berggren, E. Stavrinidou, S. Inal, I. McCulloch, *Adv. Mater.* **2020**, *2002748*, 1.
[6] A. Savva, R. Hallani, C. Cendra, J. Surgailis, T. C. Hidalgo, S. Wustoni, R. Sheelamanthula, X. Chen, M. Kirkus, A. Giovannitti, A. Salleo, I. McCulloch, S. Inal, *Adv. Funct. Mater.* **2020**, *30*, 1907657.
[7] M. Moser, L. R. Savagian, A. Savva, M. Matta, J. F. Ponder, T. C. Hidalgo, D. Ohayon, R. Hallani, M. Reisjalali, A. Troisi, A. Wadsworth, J. R. Reynolds, S. Inal, I. McCulloch, *Chem. Mater.* **2020**, *32*, 6618.
[8] D. A. Bernards, G. G. Malliaras, *Adv. Funct. Mater.* **2007**, *17*, 3538.
[9] D. Khodagholy, T. Doublet, P. Quilichini, M. Gurfinkel, P. Leleux, A. Ghestem, E. Ismailova, T. Hervé, S. Sanaur, C. Bernard, G. G. Malliaras, *Nat. Commun.* **2013**, *4*, 1575.
[10] A. Michalska, A. Gałuszkiewicz, M. Ogonowska, M. Ocypa, K. Maksymiuk, *J. Solid State Electrochem.* **2004**, *8*, 381.
[11] G. Méhes, A. Roy, X. Strakosas, M. Berggren, E. Stavrinidou, D. T. Simon, *Adv. Sci.* **2020**, *7*, 2000641.

© 2021 Wiley-VCH GmbH

[12] O. Parlak, S. T. Keene, A. Marais, V. F. Curto, A. Salleo, *Sci. Adv.* **2018**, *4*, eaar2904.
[13] J. Gladisch, E. Stavrinidou, S. Ghosh, A. Giovannitti, M. Moser, I. Zozoulenko, I. Mcculloch, M. Berggren, **2019**, *7*, 1901144.
[14] D. Moia, A. Giovannitti, A. A. Szumska, I. P. Maria, E. Rezasoltani, M. Sachs, M. Schnurr, P. R. F. Barnes, I. McCulloch, J. Nelson, *Energy Environ. Sci.* **2019**, *12*, 1349.
[15] L. Torsi, M. Magliulo, K. Manoli, G. Palazzo, *Chem. Soc. Rev.* **2013**, *42*, 8612.
[16] Y. Van De Burgt, E. Lubberman, E. J. Fuller, S. T. Keene, G. C. Faria, S. Agarwal, M. J. Marinella, A. Alec Talin, A. Salleo, *Nat. Mater.* **2017**, *16*, 414.
[17] D. Khodagholy, J. Rivnay, M. Sessolo, M. Gurfinkel, P. Leleux, L. H. Jimison, E. Stavrinidou, T. Herve, S. Sanaur, R. M. Owens, G. G. Malliaras, *Nat. Commun.* **2013**, *4*, 2133.
[18] L. Guan, L. Yu, G. Z. Chen, *Electrochim. Acta* **2016**, *206*, 464.
[19] A. Giovannitti, R. B. Rashid, Q. Thiburce, B. D. Paulsen, C. Cendra, K. Thorley, D. Moia, J. T. Mefford, D. Hanifi, D. Weiyuan, M. Moser, A. Salleo, J. Nelson, I. McCulloch, J. Rivnay, *Adv. Mater.* **2020**, *32*, 1908047.
[20] D. Kiefer, R. Kroon, A. I. Hofmann, H. Sun, X. Liu, A. Giovannitti, D. Stegerer, A. Cano, J. Hynynen, L. Yu, Y. Zhang, D. Nai, T. F. Harrelson, M. Sommer, A. J. Moulé, M. Kemerink, S. R. Marder, I. McCulloch, M. Fahlman, S. Fabiano, C. Müller, *Nat. Mater.* **2019**, *18*, 149.
[21] S. Inal, G. G. Malliaras, J. Rivnay, *Nat. Commun.* **2017**, *8*, 1767.
[22] C. B. Nielsen, A. Giovannitti, D. T. Sbircea, E. Bandiello, M. R. Niazi, D. A. Hanifi, M. Sessolo, A. Amassian, G. G. Malliaras, J. Rivnay, I. McCulloch, *J. Am. Chem. Soc.* **2016**, *138*, 10252.
[23] M. Moser, J. F. Ponder, A. Wadsworth, A. Giovannitti, I. McCulloch, *Adv. Funct. Mater.* **2019**, *29*, 1807033.
[24] J. Rivnay, P. Leleux, M. Sessolo, D. Khodagholy, T. Hervé, M. Fiocchi, G. G. Malliaras, *Adv. Mater.* **2013**, *25*, 7010.
[25] J. Rivnay, P. Leleux, M. Ferro, M. Sessolo, A. Williamson, D. A. Koutsouras, D. Khodagholy, M. Ramuz, X. Strakosas, R. M. Owens, C. Benar, J. M. Badier, C. Bernard, G. G. Malliaras, *Sci. Adv.* **2015**, *1*, e1400251.
[26] V. Kaphle, P. R. Paudel, D. Dahal, R. K. Radha Krishnan, B. Lüssem, *Adv. Funct. Mater.* **2021**, *31*, 2004939.
[27] W. Lee, D. Kim, N. Matsuhisa, M. Nagase, M. Sekino, G. G. Malliaras, T. Yokota, T. Someya, *Proc. Natl. Acad. Sci. U. S. A.* **2017**, *114*, 10554.
[28] M. Braendlein, T. Lonjaret, P. Leleux, J. M. Badier, G. G. Malliaras, *Adv. Sci.* **2017**, *4*, 1600247.
[29] M. Braendlein, A.-M. Pappa, M. Ferro, A. Lopresti, C. Acquaviva, E. Mamessier, G. G. Malliaras, R. M. Owens, *Adv. Mater.* **2017**, *29*, 1605744.
[30] A. M. Pappa, D. Ohayon, A. Giovannitti, I. P. Maria, A. Savva, I. Uguz, J. Rivnay, I. McCulloch, R. M. Owens, S. Inal, *Sci. Adv.* **2018**, *4*, eaat0911.
[31] D. A. Bernards, D. J. MacAya, M. Nikolou, J. A. Defranco, S. Takamatsu, G. G. Malliaras, *J. Mater. Chem.* **2008**, *18*, 116.
[32] H. Tang, P. Lin, H. L. W. Chan, F. Yan, *Biosens. Bioelectron.* **2011**, *26*, 4559.
[33] S. Y. Yang, F. Cicoira, R. Byrne, F. Benito-Lopez, D. Diamond, R. M. Owens, G. G. Malliaras, *Chem. Commun.* **2010**, *46*, 7972.
[34] D. Ohayon, G. Nikiforidis, A. Savva, A. Giugni, S. Wustoni, T. Palanisamy, X. Chen, I. P. Maria, E. Di Fabrizio, P. M. F. J. Costa, I. Mcculloch, S. Inal, *Nat. Mater.* **2019**, *19*, 456.
[35] E. Macchia, R. A. Picca, K. Manoli, C. Di Franco, D. Blasi, L. Sarcina, N. Ditaranto, N. Cioffi, R. Österbacka, G. Scamarcio, F. Torricelli, L. Torsi, *Mater. Horiz.* **2020**, *7*, 999.
[36] R. A. S. Luz, A. R. Pereira, J. C. P. de Souza, F. C. P. F. Sales, F. N. Crespilho, *ChemElectroChem* **2014**, *1*, 1751.
[37] R. Pauliukaite, A. Malinauskas, G. Zhylyak, U. E. Spichiger-Keller, *Electroanalysis* **2007**, *19*, 2491.
[38] S. P. White, K. D. Dorfman, C. D. Frisbie, *Anal. Chem.* **2015**, *87*, 1861.
[39] S. Lai, M. Demelas, G. Casula, P. Cosseddu, M. Barbaro, A. Bonfiglio, *Adv. Mater.* **2013**, *25*, 103.
[40] C. Napoli, S. Lai, A. Giannetti, S. Tombelli, F. Baldini, M. Barbaro, A. Bonfiglio, *Sensors* **2018**, *18*, 990.
[41] Y. Ishige, M. Shimoda, M. Kamahori, *Biosens. Bioelectron.* **2009**, *24*, 1096.
[42] M. Kamahori, Y. Ishige, M. Shimoda, *Biosens. Bioelectron.* **2007**, *22*, 3080.
[43] E. Macchia, P. Romele, K. Manoli, M. Ghittorelli, M. Magliulo, Z. M. Kovács-Vajna, F. Torricelli, L. Torsi, *Flexible Printed Electron.* **2018**, *3*, 034002.
[44] M. Yano, K. Koike, K. Mukai, T. Onaka, Y. Hirofuji, K. I. Ogata, S. Omatu, T. Maemoto, S. Sasa, *Phys. Status Solidi A* **2014**, *211*, 2098.
[45] W. Chen, S. Cai, Q. Q. Ren, W. Wen, Y. Di Zhao, *Analyst* **2012**, *137*, 49.
[46] H. Sies, *Redox Biol.* **2017**, *11*, 613.
[47] R. Wilson, Q. Elizabeth, *Biosens. Bioelectron.* **2016**, *5663*, 165.
[48] M. Seki, K. I. Iida, M. Saito, H. Nakayama, S. I. Yoshida, *J. Bacteriol.* **2004**, *186*, 2046.
[49] L. Fu, J. Liu, Z. Hu, M. Zhou, *Electroanalysis* **2018**, *30*, 2535.
[50] C. Chen, Q. Xie, D. Yang, H. Xiao, Y. Fu, Y. Tan, S. Yao, *RSC Adv.* **2013**, *3*, 4473.
[51] N. C. Foulds, C. R. Lowe, *J. Chem. Soc., Faraday Trans. 1* **1986**, *1*, 1259.
[52] B. Oktay, S. Demir, N. Kayaman-Apohan, *ChemistrySelect* **2019**, *4*, 6055.

© 2021 Wiley-VCH GmbH